HAL
archives-ouvertes.fr

Performance of an electromagnetic lead/scintillating-fibre calorimeter for the H1 detector

E. Tomasi, T. Hajduk, L. Janczur, W. Rybicki, K. Claxton, B. Dowdell, J. Deckers, H. Deckers, T. Dirkmann, M. Htte, et al.

▶ To cite this version:

HAL Id: in2p3-00013129

http://hal.in2p3.fr/in2p3-00013129

Submitted on 23 Mar 1999

Performance of an Electromagnetic Lead/Scintillating-Fibre Calorimeter for the H1 Detector

H1 SPACAL GROUP

Performance of an Electromagnetic Lead/Scintillating-Fibre Calorimeter for the H1 Detector

H1 SPACAL GROUP

Abstract

The properties of final modules of a high resolution lead/scintillating-fibre calorimeter to upgrade the backward region of the H1 detector were studied with electrons in the energy range from 2–60 GeV. The electromagnetic calorimeter consists of scintillating fibres with a diameter of 0.5 mm embedded in a lead matrix. This small fibre radius, in combination with a lead-to-fibre ratio of 2.27:1, ensures excellent energy resolution which has been measured to be $\sigma/E = 7.1\%/\sqrt{E/\mathrm{GeV}} \oplus 1.0\%$. The spatial resolution as a function of energy for impact points at the center of a cell is given by $4.4\,\mathrm{mm}/\sqrt{E/\mathrm{GeV}} + 1.0\,\mathrm{mm}$. The time resolution was found to be better than 0.4 ns.

T. Nicholls

School of Physics and Space Research, University of Birmingham, Birmingham, UK[1]

L. Hajduk, W. Janczur, K. Rybicki

Institute for Nuclear Physics, Cracow, Poland[2]

B. Claxton, J. Dowdell

Electronics Division, Rutherford Appleton Laboratory, Chilton, Didcot, UK[1]

H. Deckers, T. Deckers, M. Dirkmann, M. Hütte, H. Hutter, H. Kolanoski,
R. Pöschl, A. Schuhmacher, K. Wacker, A. Walther, D. Wegener, T. Wenk

Institut für Physik, Universität Dortmund, Dortmund, Germany[3]

G. Cozzika, B. Laforge, J.-F. Laporte, E. Perez, C. Royon, G. Villet

CEA, DSM/DAPNIA, CE-Saclay, Gif-sur-Yvette, France

R.D. Appuhn, C. Arndt, R. Barschke, R. Buchholz, U. Goerlach, V. Korbel
F. Lehner, A. Meyer, G. Müller, H. Steiner[a], M. Weber

DESY, Hamburg, Germany[3]

J. Ferencei, J. Janoth, K. Meier, S. Schleif, J. Stiewe, K. Zuber

Institut für Hochenergiephysik, Universität Heidelberg, Heidelberg, Germany[3]

W.D. Dau

Institut für Reine und Angewandte Kernphysik, Universität Kiel, Kiel, Germany[3] D. Bruncko,

F. Krivan, R. Maracek, P. Murin, J. Spalek

Institute of Experimental Physics, Slovak Academy of Sciences, Košice, Slovak Republik[4]

E. Eisenhandler, M. Landon

Physics Department, Queen Mary and Westfield College, London, UK[1]

L. Jönsson

Physics Department, University of Lund, Sweden[5]

S. Chechelnitski, V. Efremenko, B. Fominykh, I. Gorelov,
V. Nagovizin, D. Ozerov, A. Rostovtsev, V. Shekelyan, A. Semenov,
V. Solochenko, V. Tchernyshov, A. Zhokin

Institute of Theoretical and Experimental Physics, Moscow, Russia[6]

A.N. Eliseev, L.A. Gorbov, P.A. Smirnov[4]

Lebedev Physical Institute, Moscow, Russia

F. Lamarche, A. Migliori, F. Moreau, Y. Sirois, S. Spielmann, D. VanDenPlas

LPNHE, Ecole Polytechnique, IN2P3-CNRS, Palaiseau, France

E. Barrelet, U. Bassler, S. Dagoret-Campagne, F. Descamps, D. Lacour

LPNHE, Universites Paris VI and VII, IN2P3-CNRS, Paris, France

J. Cvach, I. Herynek, J. Hladky

Institute of Physics, Czech Academy of Sciences, Praha, Czech Republic[4,7]

S. Valkar, J. Zacek

Nuclear Center, Charles University, Praha, Czech Republic[4,7]

2

1 Introduction

The H1 collaboration has upgraded the H1 detector [1] at HERA during the winter shutdown 1994-95 with a new backward calorimeter to measure the energy and impact point of scattered leptons with high precision, down to angles of 3° with respect to the beam line [2]. This gives access to a wide range of Q^2 for very low values of the Bjorken scaling variable $x(10^{-4})$ in deep inelastic scattering. Since low momentum hadrons are the most frequent particles produced in $e^{\pm}p$ scattering at low x and low Q^2 and in photoproduction events, a good separation capability between electromagnetic and hadronic showers is required. Hence a very compact and fine-grained calorimeter is needed to minimise the overlap of energy depositions, and in addition to measure the scattered leptons down to small angles without energy leakage. Excellent time resolution is necessary to suppress proton-beam-induced background entering the back of the calorimeter. In addition, the calorimeter must be able to work in a magnetic field of approximately 1 Tesla and must be relatively radiation hard. The properties of final modules of our high-resolution lead/scintillating-fibre calorimeter were studied with electrons in the energy range from 2 to 60 GeV at the CERN SPS and PS, and at DESY.

1.1 Layout of the Calorimeter

To meet the requirements discussed above, the new calorimeter is divided into an electromagnetic and a hadronic section. A detailed technical description of the whole calorimeter design is given in [2, 3]. This paper is restricted to the performance of the electromagnetic section only. The space available within the existing H1 detector only allows a calorimeter with a total depth of about two hadronic interaction lengths. Since this is not sufficient to contain hadronic showers fully, there is no reason to choose a compensating design. Thus to achive the optimum energy resolution for this non-compensating electromagnetic calorimeter we chose a lead-to-fibre ratio of 2.27:1 and a fibre diameter of 0.5 mm, leading to a radiation length of 0.9 cm and a Molière radius of 2.5 cm. The basic unit of the calorimeter is a block of 52 lead plates (see figure 1) called a submodule (see figure 2) consisting of two cells each $40.5 \times 40.5 \times 250 \,\mathrm{mm}^3$. The fibres are bundled over a length of 85 mm and held in a bundling frame. At the end the fibres are glued with black glue over a length of approximately 20 mm to attenuate the light transmitted in the cladding. The fibre bundle is coupled via an air gap to a light mixer which in addition concentrates the light onto the photocathode of a $1''$ photomultiplier. The photomultiplier is glued to the light mixer. As the readout needs to be operated in a magnetic field of 1 Tesla, mesh dynode photomultipliers were chosen [4] (Hamamatsu R-5505). The spectral sensitivity of the bialkali photocathode matches the emission spectrum of blue fibres (Bicron BCF-12) which have been selected after an extensive R&D program [5]. The fibres are mirrored at their front ends with a vapourised aluminium layer, which leads to an attenuation length of approximately 3 m. Eight submodules are combined to form a supermodule of 4×4 cells, each of which has a common unit of housings for light mixers, photomutipliers, voltage dividers and cable drivers. Each unit is equipped with a high-voltage distribution board and a calibration module to monitor the gain of the photomultipliers.
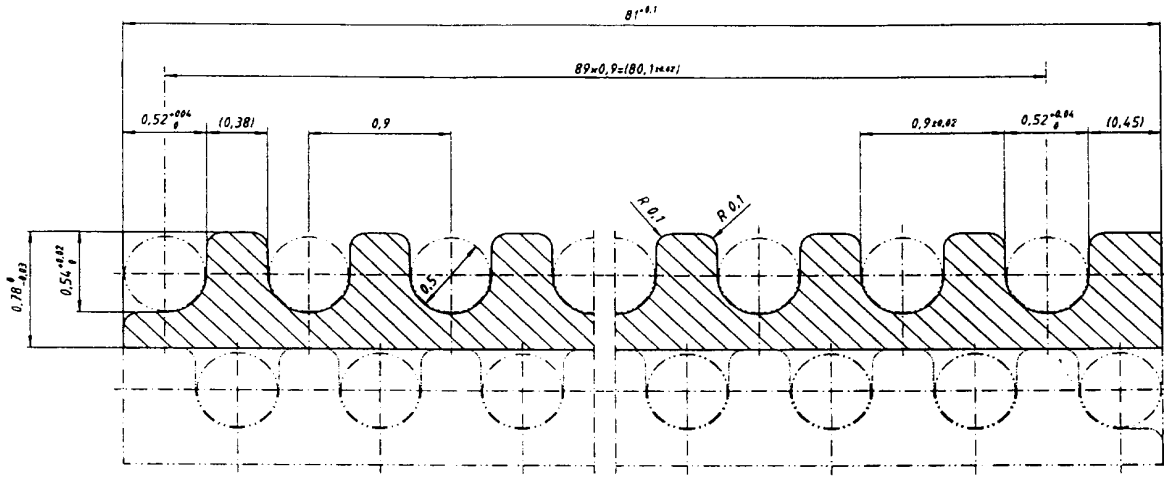
Figure 1: Front view of a lead plate with the grooves for 0.5 mm diameter scintillating fibres.
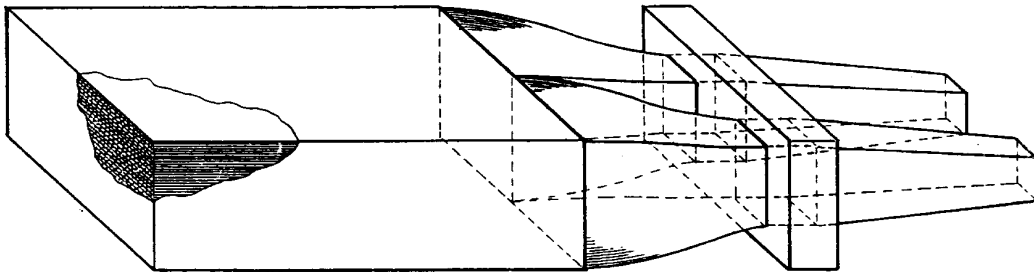

Figure 2: Schematic view of a submodule, the smallest detector unit.

2 The Experimental Set-Up and Data Processing

2.1 Set-Up and Beam-Lines

The measurements at the CERN PS were performed with four supermodules arranged as shown in figure 3 (for more details of the CERN PS test set-up see [6]). At DESY and at the CERN SPS three supermodules were tested, together with two quarters of the special insert module designed to fit around the beam-pipe (figure 4). In addition, nine modules of the hadronic calorimeter were mounted behind the electromagnetic section at the CERN PS and SPS. For all measurements the modules were mounted on horizontally and vertically movable tables.

In order to avoid the dangerous "channelling effects" which occur if fibres or lead sheets are aligned with the particle trajectory the modules were rotated by 3° (SPS and DESY) and 4.5° (PS) in the horizontal and vertical direction with respect to the beam line. These "channelling effects" were observed not only for incident tracks being parallel to the fibres but also in cases

where the projection of the incident particle track is parallel to the symmetry axes of the fibre structure (azimutal angles $\phi = 0°, 60°, 120°, ...$). Using a prototype of the calorimeter described above, we have observed a broadening of the measured energy distribution of up to 100% for 40 GeV electrons at a polar angle of 3.5° and an azimuthal angle $\phi = 60°$. The effect was visible over a range of roughly 6°. For the final detector the orientation of a submodule in a supermodule is either horizontal or vertical to avoid the effects discussed above.

At each test beam, wire chambers were mounted in front of the detectors which allowed the impact point on the calorimeter surface to be determined with a precision of 200 μm [7]. At the SPS and PS, Čerenkov counters were used to separate electrons from hadrons. The DESY test beam is a pure electron beam providing electrons between 1 and 6 GeV.

2.2 Trigger and Readout

The trigger was generated by scintillation-counter coincidences which restrict the beam spot to $10 \times 10 \, \text{mm}^2$. Additional calibration and random triggers were generated to record calibration data and pedestals. For the CERN SPS and DESY measurements the signals from the photomultipliers were digitised by LeCroy 2282 charge ADCs, and at the SPS LeCroy 2228 TDCs were used to measure the timing properties of the calorimeter. The wire chamber signals were
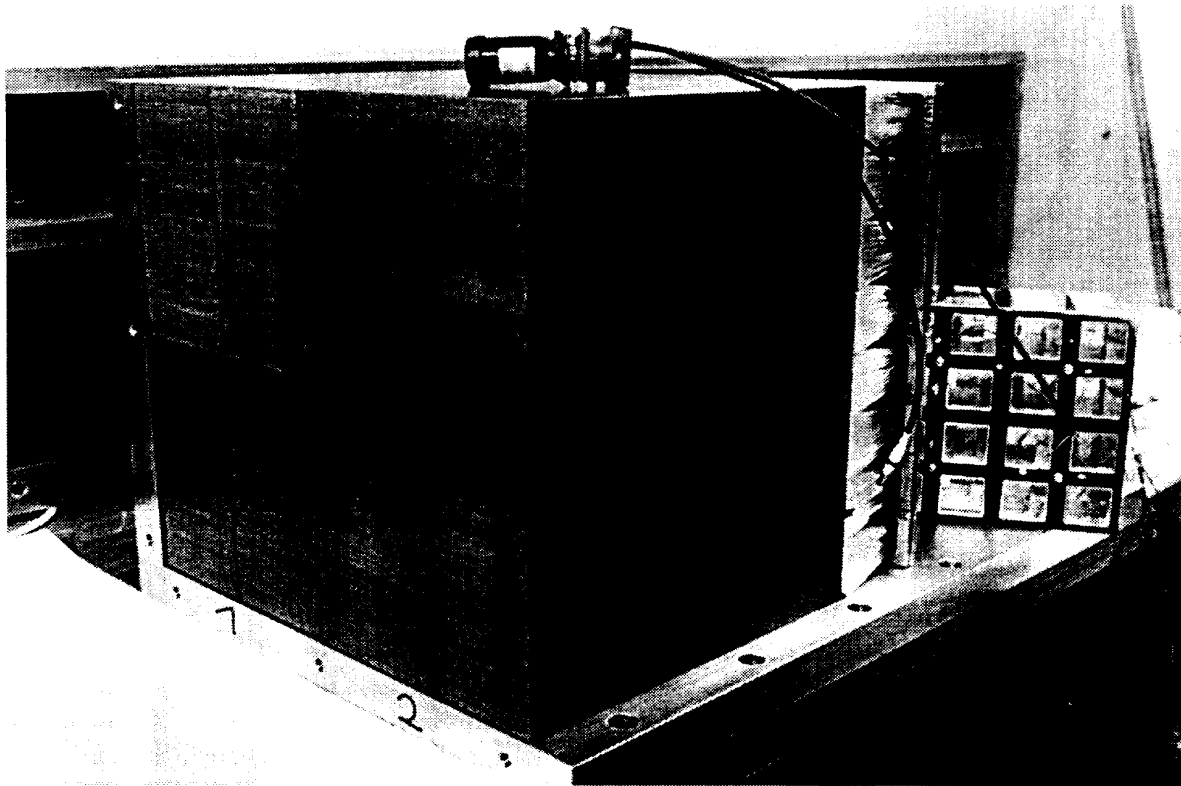

Figure 3: Photo of an array of four supermodules (64 cells) with a photomultiplier and part of the housing with light mixers as used at the CERN PS.

fed into LeCroy 2228 TDCs. The ADCs and TDCs were read out by a VME computer running the CERN Spider data acquisition suite under the OS9 operating system. The complete set-up of all counters for the CERN SPS measurements is shown in figure 5. At the DESY test beam no spectrometer and no Čerenkov counters were used. At the CERN PS a prototype of the final readout electronics was used [2, 6] to measure the timing properties of the calorimeter using a constant-fraction discriminator.

2.3 Calibration

The individual cells of the detector were calibrated with electrons of fixed energy shot into the centre of each cell. Off-line, the calibration constants (the relation between collected charge in ADC counts and energy) were determined from this data. To monitor instabilities of the photomultiplier gain, we used a Xenon flashlamp together with a reference photomultiplier and an α-source ($^{241}_{95}$Am) to calibrate the flashlamp signals. The signals were fed by plastic optical fibres into the light mixers in front of the photomultipliers. Using this system we obtained a relative cell-to-cell calibration of better than 2%. In the H1 detector the calorimeter will be monitored by an LED calibration system [2].
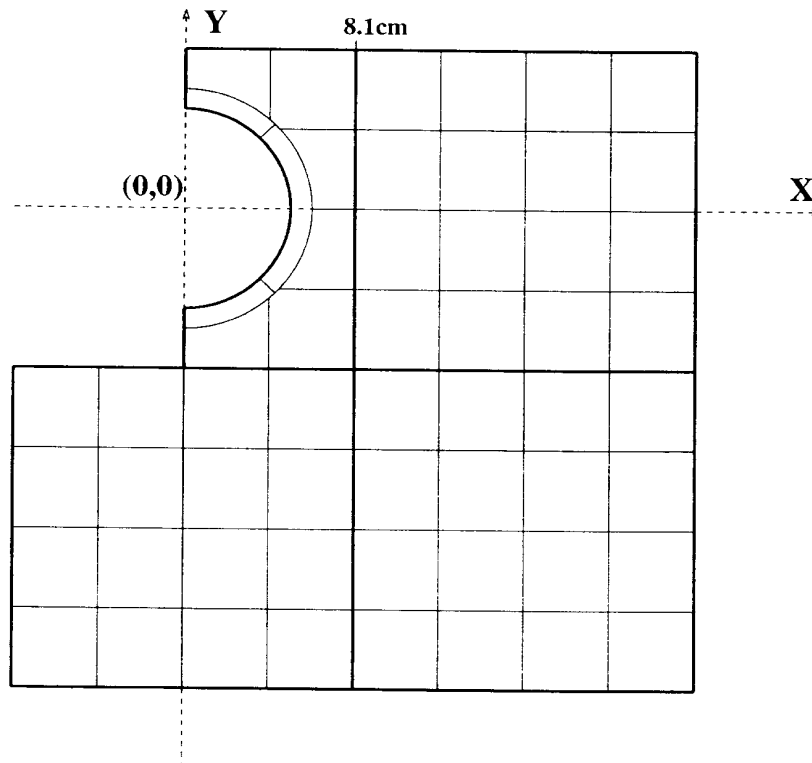

Figure 4: Schematic view of the detector set-up for the CERN SPS and DESY measurements.
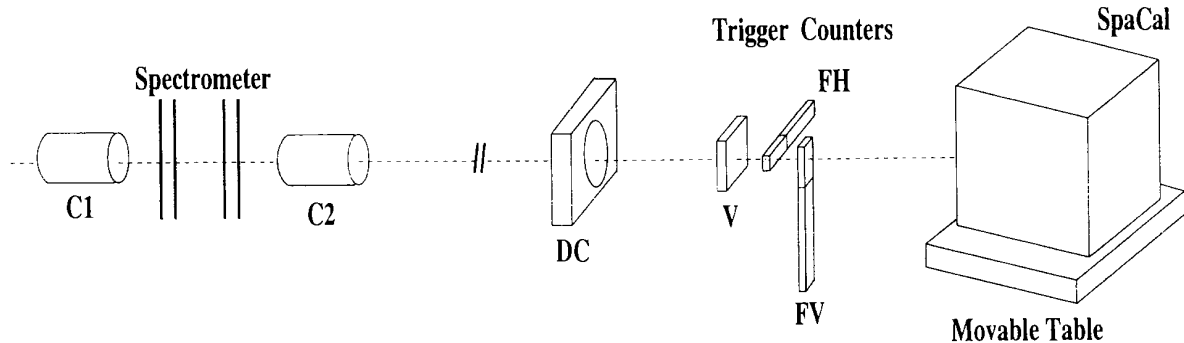
Figure 5: Schematic view of beam line for the SPS measurements. C1 and C2 are two Čerenkov counter; DC is the drift chamber used for track determination; FH and FV are the horizontal and vertical finger counters: V is an additional scintillation-counter of $5 \times 5 \, \mathrm{cm}^2$

3 Results from the Measurements

3.1 Homogeneity and Linearity

The lead/fibre matrix of the calorimeter is very homogeneous, as can be seen from figure 3. The borders between the supermodules are clearly visible due to small shifts caused by the stacking procedure. However, this should have no influence on the response to energetic showering electrons.

Figure 6 shows the response of different cells together with the sum of the cell signals obtained from a horizontal scan with 4 GeV electrons at the CERN PS. The scan shows signal losses of up to 8% at the borders of submodules compared to the maximum response of the calorimeter. The reduction of the response is much smaller at the boundary between two cells within one submodule. Additional scans using different modules and scanning at various vertical and horizontal positions have shown that the inhomogeneities mainly occur at submodule boundaries. However, the size of the signal losses varies widely between 0% and 8%. Thus, the example shown is the worst case we can expect in our calorimeter.

The most probable explanation for these inhomogeneities is damage to the fibres at the border of submodules because the submodules are pressed to their nominal dimensions using a total pressure of 1.5 tonnes. This pressure is equivalent to the pressure caused by the weight of the calorimeter in the final assembly. In figure 1 one can imagine that the right outermost fibre in the lower lead plate has no side support, and thus can be damaged by the lead above if pressure is applied to the module. Monte Carlo simulations have shown that a signal reduction of one to two layers of border fibres to approximately 50% of the nominal light output can explain the inhomogeneities observed in the test measurements. As the damage to the fibres is very sensitive to the fibre radius, the dimensions of the lead plate and the pressurisation process, the large variations of the signal losses for different modules can easily be understood.

The linearity of the calorimeter was measured at the CERN SPS between 10 and 60 GeV. Taking the beam momentum resolution into account we measured a maximum deviation from linearity of 1.3%, which is within the nonlinearities of our readout electronics.

A dedicated run in which we shot the beam into the calorimeter was used to measure the
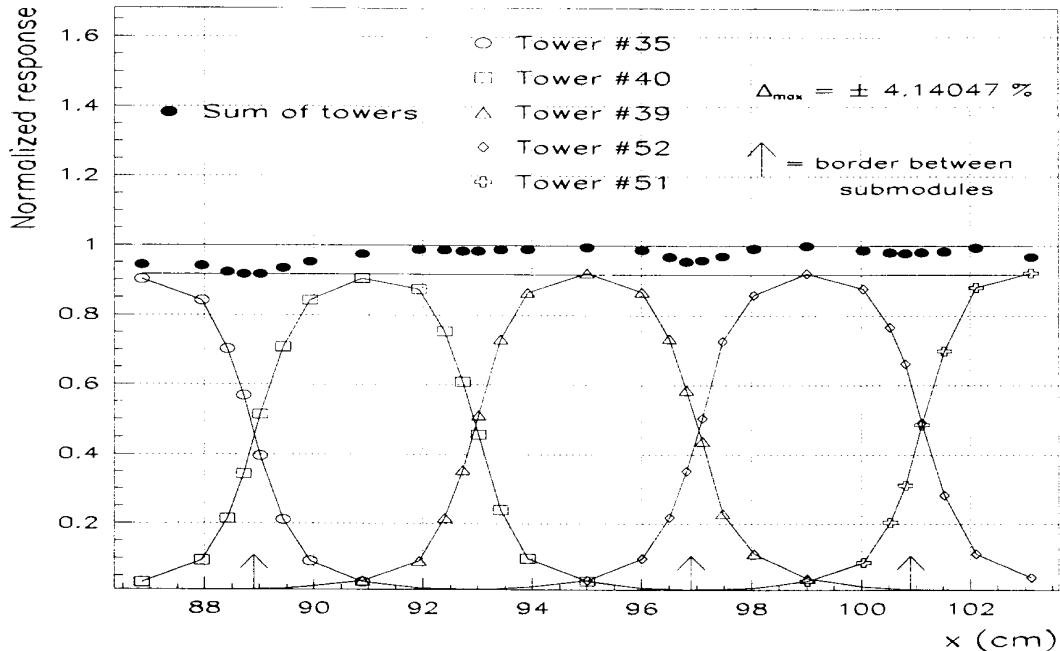
8

Figure 6: Vertical scan across five calorimeter cells together with the sum of these cells.

leakage of the electromagnetic section by analysing the response of the calibrated hadronic section. We found that the longitudinal losses are of the order of 40 MeV for electron energies of 45 GeV. In addition, the energy measured in the hadronic section shows a strong positive correlation with the energy measured in the electromagnetic section against a naive expectation. The reason for this is the energy deposition in the fibre bundles which increases with increasing leakage leading to a larger signal of the electromagnetic section. These results show that longitudinal losses are not critical in this 28 X_0-long calorimeter, and that the attenuation length of the fibres is long enough to avoid nonlinearities due to the longitudinal movement of the shower maximum as a function of energy.

3.2 Energy Resolution

For this analysis we combine the CERN SPS and DESY measurements, where the same modules were used. Figure 7 shows the ADC sum of nine calibrated cells for electron energies between 10 and 60 GeV. The mean values and the widths of Gaussian fits are used in the following comparisons. For these resolution measurements only impact points on the calorimeter surface where the inhomogeneities mentioned above are small were used.

In figure 8 the normalised resolution σ/E is plotted versus $1/\sqrt{E}$. For the DESY measurements the estimated beam resolution of 85 MeV [12] was subtracted in quadrature from the data, while the momentum smearing of the CERN SPS beam contributes to the apparent constant term of the energy resolution.
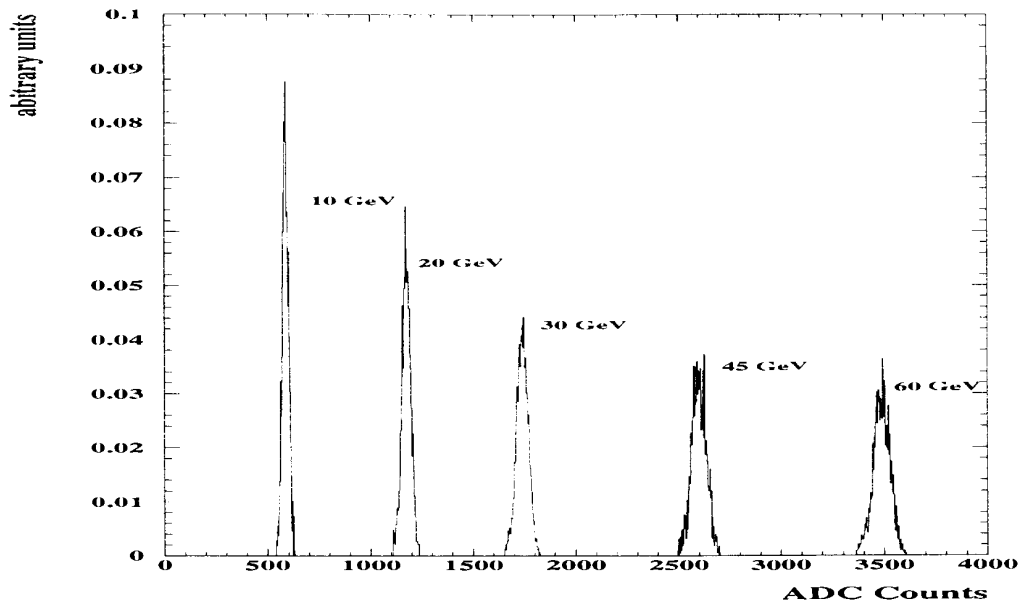
Figure 7: Pedestal subtracted signals for electrons of 10 to 60 GeV. All distributions are normalised to the same area.
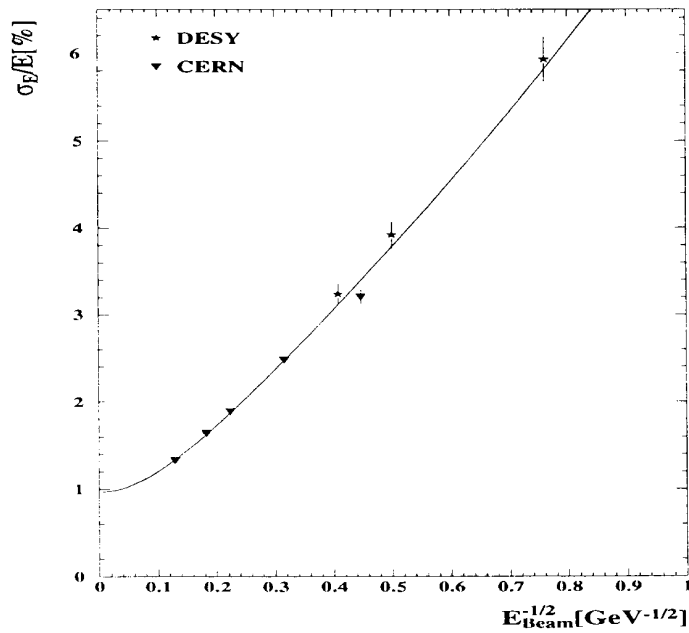

Figure 8: The energy resolution of the calorimeter as measured at DESY and CERN SPS.

We analysed the energy resolution using:

$$\frac{\sigma}{E} = \frac{a}{\sqrt{E}} \oplus \frac{b}{E} \oplus c.$$

The result of the fit shows that the noise term is negligible. Thus the final resolution can be parametrised by

$$\frac{\sigma}{E} = \frac{(7.1 \pm 0.2)\%}{\sqrt{E/\mathrm{GeV}}} \oplus (1.0 \pm 0.1)\%.$$

Our measurements of the light yield of the fibres, together with Monte Carlo simulations, show that a constant term of 0.5% is due to light-yield fluctuations of the fibres. The result of the sampling term is in good agreement with extrapolations based on the fibre radius and lead-to-fibre volume ratio [8], and with Monte Carlo studies using a detailed description of the calorimeter in EGS [9] yielding a sampling term of 7.2%.

The overall constant term of the whole calorimeter will be larger than the number derived from the fit due to the inhomogeneities of the calorimeter. To estimate this contribution we used a Monte Carlo simulation parametrising the signal losses at all submodule boundaries by a gaussian of width 2.5 mm (sigma) and of depth 5%. This simulation predicts a constant term of 2.2%.

3.3 Position Resolution

We calculated the impact points of electromagnetic showers from the energy seen in the cells by using a logarithmic weighting method [10]: $\bar{r} = \sum_i w_i r_i / \sum_i w_i$, where r_i denote the centre coordinates of the cells and the weights w_i were calculated from the energies E_i detected in each cell by $w_i = max(0, w_o + ln(E_i / \sum_j E_j))$. The optimum choice of w_0 depends on the impact energy, the cell size and the impact angle. Fortunately, the energy dependence of w_0 is weak. Thus for fixed impact angle the parameter w_0 is determined by the cell size only. Figure 9 shows the spatial resolution of the calorimeter for 4 GeV electrons from the CERN PS as function of w_0. A broad plateau with a minimum at $w_0 = 4.3$ is clearly visible. This optimal value for w_0 was confirmed by Monte Carlo studies and is used to calculate the impact point for all energies. The reconstructed impact point was then compared to the extrapolation of a track measurement by a wire chamber [7] in front of the calorimeter. The extrapolation determined the impact point on the calorimeter surface with a resolution of 200 μm in both the vertical and horizontal planes. For 4 GeV electrons, figure 10 shows the impact position calculated from the energy depositions in the calorimeter versus the extrapolation from the chamber. The superimposed straight-line fit indicates that the impact point reconstruction shows no non-linearities over the whole cell area. This is not the case if, for example, a linear weighting method is used.

Figure 11 shows the resolution achieved for two different impact points. The resolution obtained from a Gaussian fit to the impact point distribution is significantly better if the beam hits the calorimeter just between two cells compared to an impact position in the centre of a cell, because in the former case the energy is equally shared between the cells. In figure 12 the resolution for two different impact points is plotted versus the beam energy. Fitting these two curves we obtained a spatial resolution of

$$\sigma = (3.8 \pm 0.4)\,\mathrm{mm}/\sqrt{E/\mathrm{GeV}} + (0.3 \pm 0.2)\,\mathrm{mm}$$

for impact points at the edge of two cells, and

$$\sigma = (4.4 \pm 0.4)\,\mathrm{mm}/\sqrt{E/\mathrm{GeV}} + (1.0 \pm 0.2)\,\mathrm{mm}$$
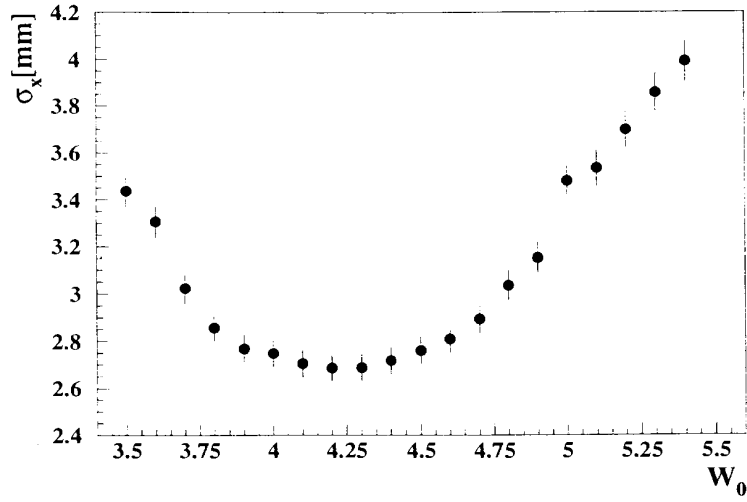
Figure 9: Determination of the optimal cut-off parameter w_0 for the reconstruction of the impact point of 4 GeV electrons.
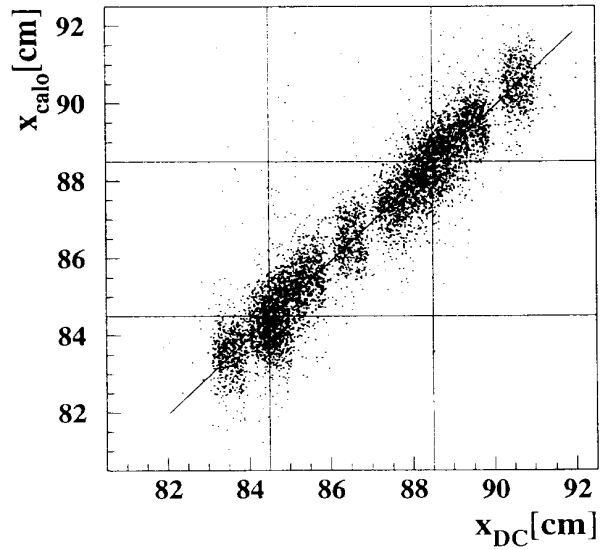

Figure 10: Impact position calculated from the energy depositions in the calorimeter versus the extrapolation from the chamber for 4 GeV electrons. The cell boundaries are indicated by full lines.

for central impact on a cell. These results are in good agreement with Monte Carlo studies [11].
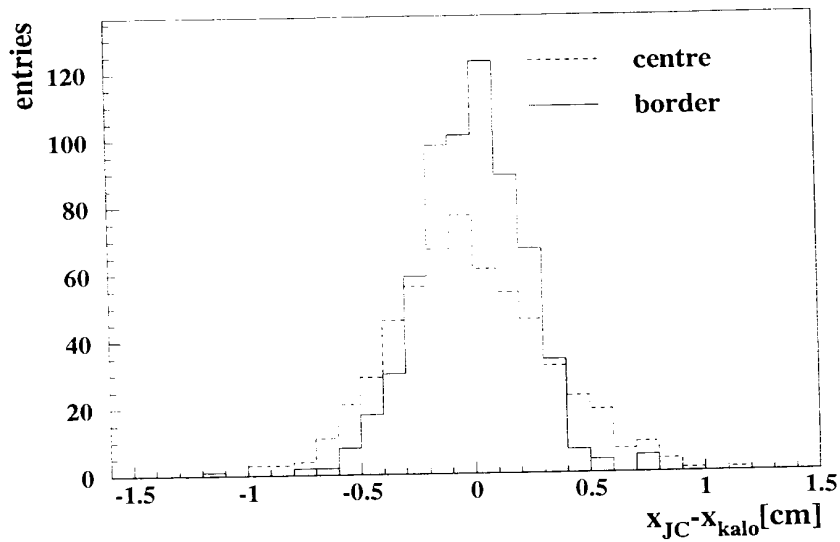
Figure 11: Spatial resolution of 4 GeV electrons hitting the calorimeter at two different impact points.
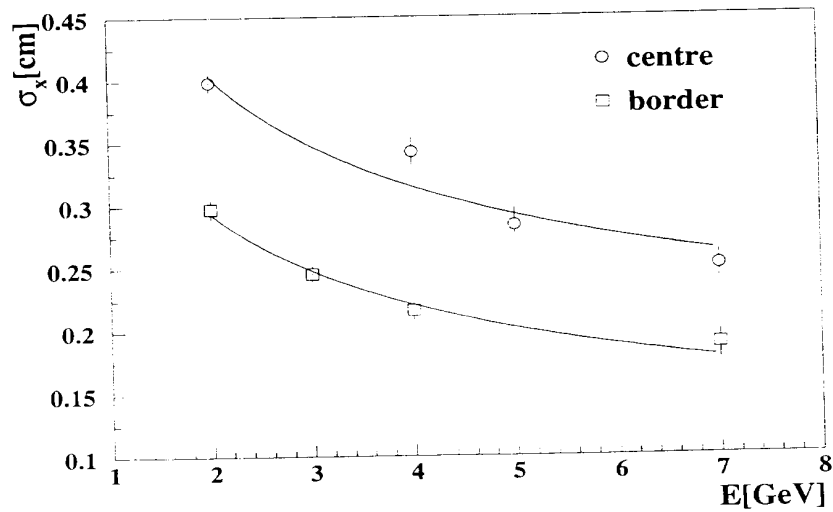

Figure 12: Energy dependence of the spatial resolution for two different impact points. The full lines are the superimposed fit results.

3.4 Time Resolution

To measure the time resolution of the calorimeter the signals of the beam-defining scintillators were connected to TDCs. At the CERN SPS two perpendicular finger counters and a paddle counter were used. The signal of the horizontal finger counter was used to generate the common start signal of the TDC.

The time resolution of the beam-defining scintillators was determined by calculating the width of the differences of their distributions. This is possible if the time resolutions of the different scintillators are nearly equal and show gaussian behaviour. Knowing the time resolution of the start signal then allows us to calculate the time resolution of the calorimeter. We find:

$$\sigma_{Cal} = (0.38 \pm 0.03)\,\mathrm{ns}.$$

This is not the intrinsic time resolution of the calorimeter, but is dominated by the time resolution of the photomultipliers [4].

At the CERN PS we used the final readout electronics to measure the time resolution as a function of the pulse height. For this measurement 4 GeV electrons, pions and muons were used. Figure 13a shows that the time resolution is nearly independent of the deposited energy if a constant-fraction discriminator is used. Fitting the projection of the time measurements, as shown in figure 13b, results in a time resolution of the whole system of $(0.82 \pm 0.01)\,\mathrm{ns}$.

In addition, it could be shown that the time resolution for particles entering the rear of the calorimeter is only 10% worse than for frontal impact. These results indicate that the calorimeter is well-suited to work as a time-of-flight system, allowing rejection of proton-induced background entering the H1 detector from upstream.

4 Summary

We have studied the properties of final modules for the new high resolution electromagnetic lead/scintillating-fibre calorimeter of the H1 detector. The main features are good energy and spatial resolution, and a very good time resolution. The small fibre radius of 0.5 mm, in combination with a lead-to-fibre ratio of 2.27:1, ensures excellent energy resolution which has been measured to $\sigma/E = (7.1 \pm 0.2)\%/\sqrt{E/\mathrm{GeV}} \oplus (1.0 \pm 0.1)\%$. The spatial resolution as function of energy for impact points at the center of a cell is given by $\sigma = (4.4 \pm 0.4)\,\mathrm{mm}/\sqrt{E/\mathrm{GeV}} + (1.0 \pm 0.2)\,\mathrm{mm}$. The time resolution was found to be better than 0.4 ns.
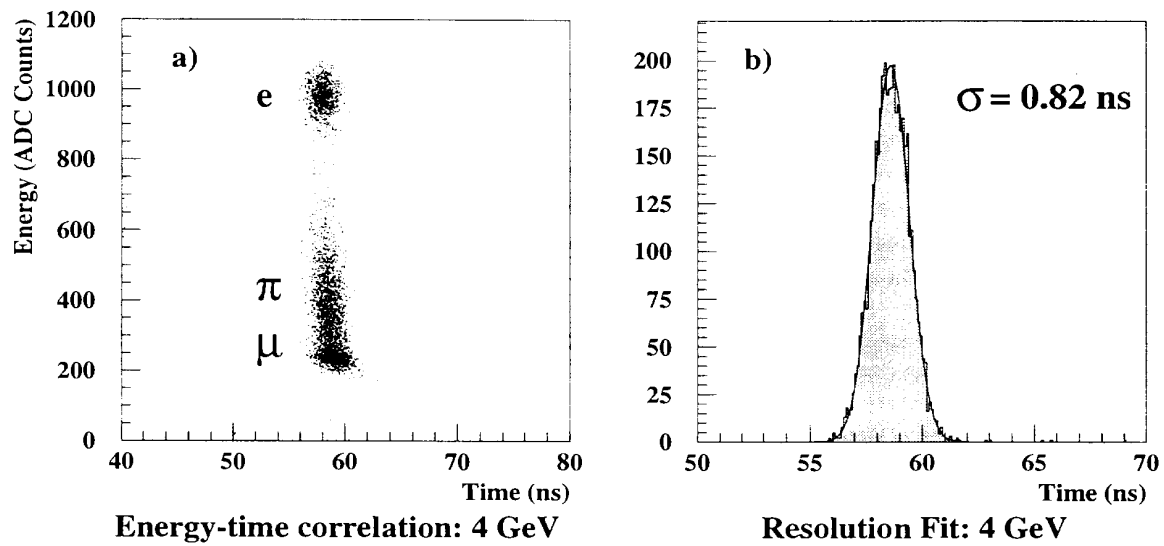
Acknowledgements

Figure 13: a) Pulse height dependence of the time measurement (the pedestal of 160 ADC counts is not subtracted) and b) time resolution obtained with the final readout electronics using 4 GeV particles.

References

[1] H1 Collaboration, *The H1 Detector at HERA*, DESY 93-103.

[2] H1 Collaboration, *Technical Proposal to Upgrade the Backward Scattering Region of the H1 Detector*, PRC 93/02, March 8, 1993.

[3] The H1 Lead/Scintillating-Fibre Calorimeter. To be submitted to NIM.

[4] Hamamatsu Photonics Data Sheet R5505;
R.D. Appuhn et al., *Performance Tests with a Large Sample of Fine Mesh Photomultipliers for Use at 1.2 Tesla*, Proceedings of the IV International Conference on Calorimetry in High Energy Physics, La Biodola, Elba, Italy (1993) 118;
J. Janoth et al., Nucl. Instr. and Meth. A350(1994) 221;
Test of a Large Number of Fine-Mesh Photomultiplier Tubes for Usage in a Magnetic Field of 1.2 Tesla, To be submitted to NIM.

[5] A. Walther and R. Barschke, *Studies of Scintillating Fibres for a Spaghetti Calorimeter to be used for the H1 Backward Upgrade Project*, Proceedings of SCIFI 93 Workshop on Scintillating Friber Dectors, Notre Dame University, Indiana, USA (1993) 253;
R. Barschke, Diploma Thesis, University of Hamburg, Germany, unpublished $(1994)^{WWW}$;
F. Lehner, Diploma Thesis, University of Hamburg, Germany, unpublished $(1994)^{WWW}$;
A. Schuhmacher, Diploma Thesis, University of Dortmund, Germany, unpublished (1994);
T. Wenk, Diploma Thesis, University of Dortmund, Germany, unpublished (1994).

[6] Hadronic Response and e/π Separation with the H1 Lead/Scintillating-Fibre Calorimeter, To be submitted to NIM.

[7] H. Deckers, Diploma Thesis, University of Dortmund, Germany, unpublished $(1994)^{WWW}$.

[8] R. Wigmans, *Performance and Limitations of Hadron Calorimetry*, CERN-PPE/91-205;
M. Livan and R. Wigmans, *Scintillating-Fibre Calorimetry*, CERN 95-02.

[9] K. Bogusch, Diploma Thesis, University of Dortmund, Germany, unpublished (1993).

[10] T.C. Awes et al., Nucl. Instr. Meth. A311(1992) 130.

[11] M. Dirkmann, Diploma Thesis, University of Dortmund, Germany, unpublished $(1995)^{WWW}$.

[12] H. Hutter, Diploma Thesis, University of Dortmund, Germany, unpublished $(1995)^{WWW}$.

^{WWW} These documents can be found on the World Wide Web.
Address: http://dice2.desy.de/h1/www/h1det/calo/spacal/pubs.html